Electrochemical Reactivity of Mg_2Sn Phases with Metallic Lithium

Dominique Larcher,* A. S. Prakash, Juliette Saint, Mathieu Morcrette, and Jean-Marie Tarascon

Laboratoire de Réactivité et Chimie des Solides, CNRS UMR 6007, Université de Picardie Jules Verne, 33 rue Saint Leu, 80039 Amiens, France

Received June 14, 2004. Revised Manuscript Received September 15, 2004

Stable (c) and metastable (h) forms of Mg_2Sn were prepared as crystallized phases by ball-milling of elemental powders. Through in situ X-ray diffraction measurements, we deduced the reactivity mechanisms of c-Mg_2Sn toward lithium. It entails first a monophasic insertion of about one lithium per formula unit into the fcc Sn framework without extrusion of either Mg or Sn, then a biphasic process leading to the formation of cubic Li_2MgSn concomitant with a progressive expulsion of Mg, and finally the formation of Li−Mg solid-solution alloys. Upon charging, the poor reversibility of the alloying reaction of Li with Mg leads to a deficit in free Mg, resulting in the formation of a Mg_2Sn + Sn mixture, and accounting for the poor cyclability of Mg_2Sn/Li cells over the 0.0−1.5 V voltage window. Limiting the cycling to the monophasic process was shown to improve the cycling behavior. Finally, we found that the electrochemical reaction of h-Mg_2Sn with Li leads to the same Li_2MgSn intermediate and the same subsequent sequence of transformations, resulting in similarly poor capacity retention upon cycling.

Introduction

For the past three decades, the alloying reaction of (semi)metals with metallic lithium has been one of the most explored approaches in the search for alternatives to carbonaceous materials as negative electrodes for Li ion batteries. To our knowledge, Dey was the first to report such electrochemical alloying with Sn, Pb, Al, Au, Pt, Zn, Cd, Ag, and Mg in organic solvent and to point out that "the alloying caused complete disintegration of the electrodes and the consequent loss of electronic contact".[1] Despite the large first discharge capacities ($Li_{4.4}Si$, 4200 (mA h)/g; $Li_{4.4}Ge$, 1620 (mA h)/g; LiAl and $Li_{4.4}Sn$, 1000 (mA h)/g) that easily exceed those of the carbonaceous materials presently commercialized (370 (mA h)/g), these alloying processes are indeed poorly reversible and rate limited. This limitation is commonly attributed to the important electrode volume changes occurring during the Li incorporation, associated with phase transitions that result in cracks and finally loss of electrical contact. To overcome this issue, many studies have been undertaken to determine whether metallic materials can host lithium without undergoing such a pulverization. This can be investigated through electrode engineering by the use of small particles that could sustain strains with less cracks,[2] the synthesis of composites where metals are embedded in either an active or an inactive matrix,[3−8] or the preparation of dense substrated films.[9−12] A last approach consisting of designing new powdered multielement alloys that could reversibly react with lithium through a displacement or intercalation process recently revealed very appealing results. Indeed, since the report by Thackeray et al.[13] of the insertion of Li into the η-Cu_6Sn_5 metallic framework, many groups randomly investigated the properties of various binary and even ternary systems.[14−18] Among them, the Li−Mg−X systems (X = Si, Ge, Sn, Pb) were recently screened and led to conflicting reports on the reaction proposed to describe the electrochemical

* To whom correspondence should be addressed. E-mail: dominique.larcher@sc.u-picardie.fr.

(1) Dey, A. N. *J. Electrochem. Soc.* **1971**, *118* (10), 1547.
(2) Yang, J.; Winter, M.; Besenhard, J. O. *Solid State Ionics* **1996**, *90*, 281.
(3) Boukamp; B. A., Lesh, G. C.; Huggins, R. A. *J. Electrochem. Soc.* **1981**, *128* (4), 725.
(4) Idota, Y.; Kabuto, T.; Matsufuji, A.; Maekawa, Y.; Miyasaki, T. *Science* **1997**, *276*, 1395.
(5) Courtney, I. A.; Dahn, J. R. *J. Electrochem. Soc.* **1997**, *144* (9), 2943.
(6) Courtney, I. A.; Dahn, J. R. *J. Electrochem. Soc.* **1997**, *144* (6), 2045.
(7) Wilson, A. M.; Dahn, J. R. *J. Electrochem. Soc.* **1995**, *142* (2), 326.
(8) Yang, J.; Wang, B. F.; Wang, K.; Liu, Y.; Xie, J. Y.; Wen, Z. S. *Electrochem. Solid-State Lett.* **2003**, *6* (8), A154.
(9) Graetz, J.; Ahn, C. C.; Yazami, R.; Fultz, B. *Electrochem. Solid-State Lett.* **2003**, *6* (9), A194.
(10) Kim, Y.-L.; Lee, H. Y.; Jang, S. W.; Lim, S. H.; Lee, S. J.; Baik, H. K.; Yoon, Y. S.; Lee, S. M. *Electrochim. Acta* **2003**, *48*, 2593.
(11) Maranchi, J. P.; Hepp, A. F.; Kumtaa, P. N. *ECS Lett.* **2003**, *6* (9), A198.
(12) Beaulieu, L. Y.; Eberman, K. W.; Krause, L. J.; Dahn, J. R. *Electrochem. Solid-State Lett.* **2001**, *4* (9), A137.
(13) Thackeray, M. M.; Vaughey, J. T.; Kahaian, A. J.; Kepler, K. D.; Benedek, R. *Electrochem. Commun.* **1999**, *1* (3−4), 111.
(14) Mao, O.; Dahn, J. R. *J. Electrochem. Soc.* **1999**, *146* (2), 414.
(15) Vaughey, J. T.; O'Hara, J.; Thackeray, M. M. *Electrochem. Solid-State Lett.* **2000**, *3* (1), 13.
(16) Fransson, L. M. L.; Vaughey, J. T.; Benedek, R.; Edstrom, K.; Thomas, J. O.; Thackeray, M. M. *Electrochem. Commun.* **2001**, *3* (7), 317.
(17) Larcher, D.; Beaulieu, L. Y.; Mao, O.; George, A. E.; Dahn, J. R. *J. Electrochem. Soc.* **2000**, *147* (5), 1703.
(18) Weydanz, W. J.; Wohlfahrt-Mehrens, M.; Huggins, R. A. *J. Power Sources* **1999**, *81−82*, 237.

10.1021/cm040132h CCC: $27.50
Published on Web 11/12/2004

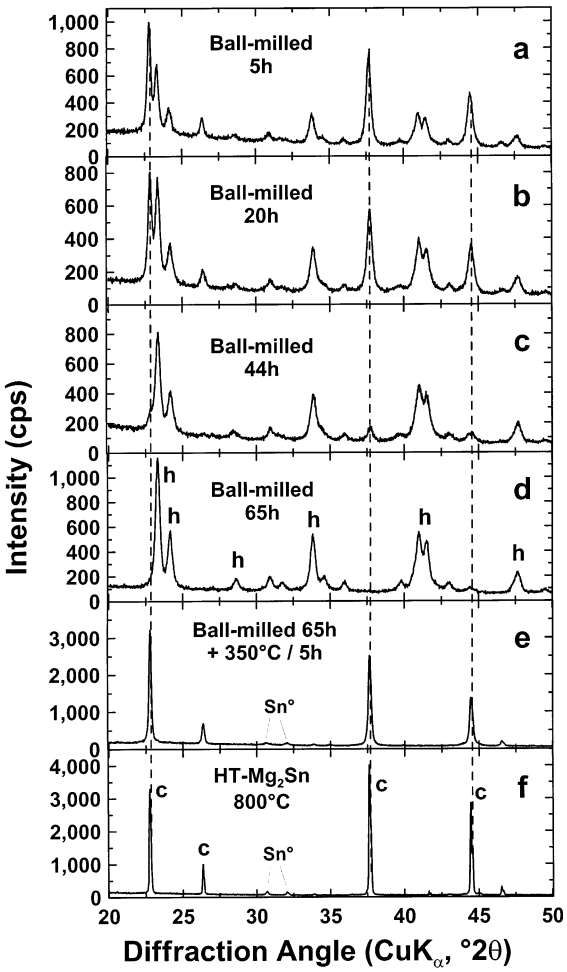

Figure 1. X-ray diffraction patterns of the materials obtained by ball-milling Mg/Sn mixtures for milling times ranging from 5 h (a) to 65 h (d), the powder obtained by heating (350 °C/vacuum/5 h) sample d (e), and the sample prepared by heating Mg/Sn mixtures in a sealed quartz tube at 800 °C (f). The h and c labels indicate the Bragg peaks of the high-pressure h-Mg_2Sn metastable and stable c-Mg_2Sn phases, respectively.

lithiation of the structurally alike cubic Mg_2X phases.[19−25] Although the formation of Li_2MgX phases ($Mg_2X + 2Li \rightarrow Li_2MgX + Mg$) is a well established and common fact, many questions still remain: the way this ternary phase is formed, its electrochemical activity and stability, the decomposition of the electrodes into Li−X alloys, the formation of Li−Mg phases, the high-voltage behaviors, etc. Among the four Li−Mg−X systems, Li−Mg−Si is the one reaching some kind of consensus, even though the question of the possible formation of Li−Si alloys remains unanswered. In contrast, the reaction of Mg_2Sn with lithium is far from being totally understood, motivating our choice in this system.[21,22,24]

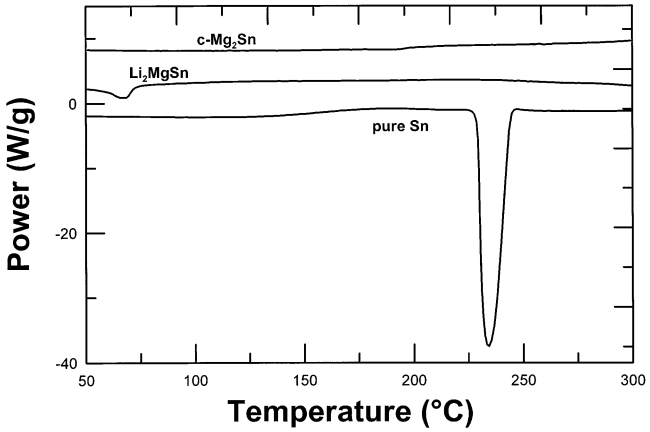

Figure 2. DSC curves for c-Mg_2Sn (sample e, Figure 1), ternary Li_2MgSn, and pure Sn as reference (heating rate 5 °C/min, argon flow).

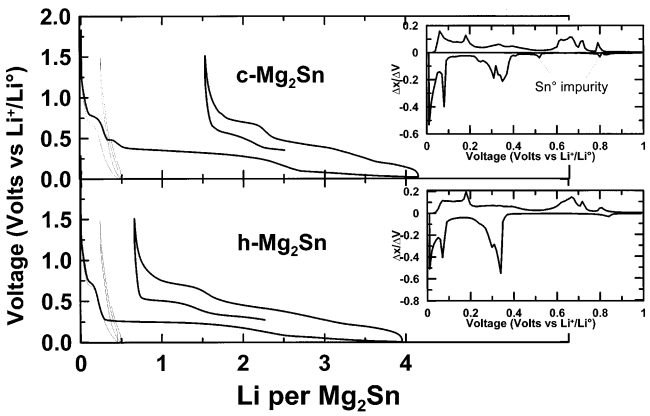

Figure 3. Voltage−composition curves for c-Mg_2Sn/Li and h-Mg_2Sn/Li cells recorded in galvanostatic mode at a rate of 1 Li atom in 5 h at 20 °C. The equivalent contribution of the conducting SP carbon was computed and superimposed to visualize its contribution to the overall capacity. The insets display the incremental dx/dV capacities obtained by integration of the chronoamperometric titration curves for both samples (step 10 mV, equivalent cutoff current C/20).

In this paper, we will therefore present the electrochemical reactions occurring in Mg_2Sn/Li cells upon cycling and will exemplify that a dense metallic framework can be extremely stable upon exchange or insertion reaction. Along that line, we show, for instance, that cubic Mg_2Sn can host lithium without any extrusion of Sn or Mg, that Li−Mg alloys are irreversibly produced, and that free Sn can be expulsed from the structure without giving rise to Li−Sn alloys.

Experimental Section

Binary (Mg−Sn) and ternary (Li−Mg−Sn) materials were prepared by reacting stoichiometric amounts of elemental metallic powders (purity >99%) through a ball-milling process. Typically, for such a synthesis, 2 g of the mixed powders and a steel ball (7 g) were loaded into a stainless steel vial under an argon atmosphere. Then, the sealed vial was sequentially shaken for various lengths of time in an SPEX8000 miller with 15 min of interruption every 30 min of shaking to release as much as possible of the shock-induced generated heat. A batch of cubic Mg_2Sn (noted HT-Mg_2Sn) was also prepared by heating a powdered Sn/Mg mixture in a sealed tube, under argon, at 800 °C for 1 day.

The morphology and elemental and phase compositions of the so-obtained powders were regularly checked by scanning

(19) Kim, H.; Choi, J.; Sohn, H.; Kang, T. *J. Electrochem. Soc.* **1999**, *146* (12), 4401.
(20) Moriga, T.; Watanabe, K.; Tsuji, D.; Massaki, S.; Nakabayashi, I. *J. Solid State Chem.* **2000**, *153* (2), 386.
(21) Sakaguch, H.; Maeta, H.; Kubota, M.; Honda, H.; Esaka, T. *Electrochemistry* **2000**, *68* (8), 632.
(22) Kim, H.; Kim, Y. J.; Kim, D. G.; Sohn, H. J.; Kang, T. *Solid State Ionics* **2001**, *144* (1−2), 41.
(23) Roberts, G. A.; Cairns, E. J.; Reimer, J. A. *J. Power Sources* **2002**, *110* (2), 424.
(24) Roberts, G. A.; Cairns, E. J.; Reimer, J. A. *J. Electrochem. Soc.* **2003**, *150* (7), A912.
(25) Roberts, G. A.; Cairns, E. J.; Reimer, J. A. *J. Electrochem. Soc.* **2004**, *151* (4), A493.

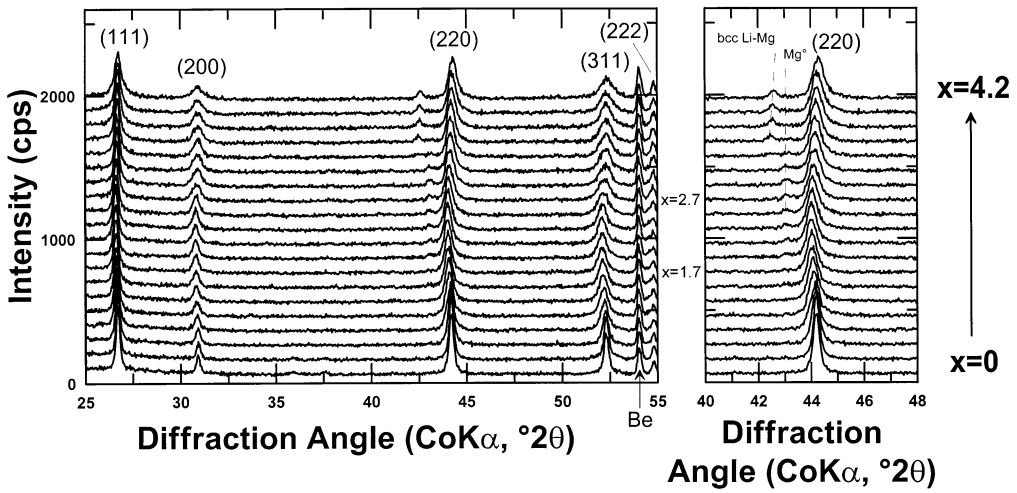

Figure 4. Evolution of the XRD patterns along the discharge of a c-Mg_2Sn/Li cell at 1 Li atom in 5 h at 20 °C. The beryllium peak is due to the airtight sample holder.

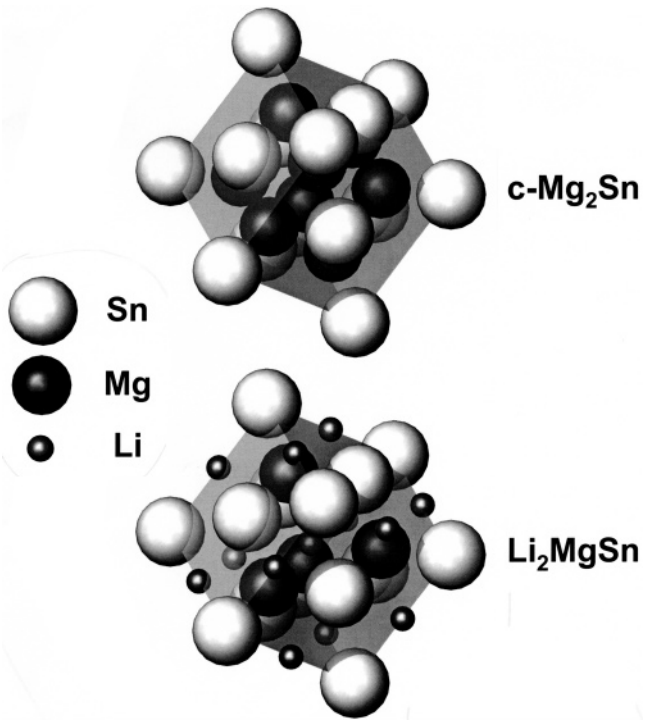

Figure 5. Representation of the structural unit cells for c-Mg_2Sn and Li_2MgSn based on data in refs 35 and 36, respectively.

electron microscopy (SEM) (Philips SEM FEG XL 30), energy dispersive spectroscopy (EDS) analysis (Link Isis Oxford), and X-ray diffraction (XRD), respectively. Two diffractometers were used, a Siemens D8 (Co Kα, $\lambda = 1.79026$ Å, $\theta-\theta$ geometry, position-sensitive detector) for in situ experiments and a Scintag PAD V (Cu Kα, $\lambda = 1.5408$ Å) for regular powder analyses. Peak fwhm's (full widths at half-maximum) were evaluated by fitting the diffraction peaks with a pseudo-Voigt profile.

Thermal analysis (TGA, thermogravimetric analysis; DSC, differential scanning calorimetry) curves were collected on a Mettler apparatus at a heating rate of 5 °C/min under static air or argon flow. Specific surface areas were determined from the results of N_2 physisorption at 77 K with a 2375 Gemini analyzer using the BET multipoint method.[26] The samples were preheated under argon flow for 1 h at 150 °C.

For in situ experiments and XRD analysis of air-sensitive samples, a modified Swagelok cell was equipped with a thin beryllium window acting as a current collector.[27] X-ray scans were recorded at ambient temperature while the in situ cells were continuously discharged/charged at a rate of 1 Li atom in 5 h without current relaxations.

Electrodes were typically prepared by mixing 85 wt % active material and 15 wt % SP carbon as the electronic conductor. Swagelok-type cells were assembled in an argon-filled glovebox with about 10 mg of the carbon/active material mixture separated from a lithium foil by two sheets of fiberglass disks, the whole being soaked in an ethylene carbonate/dimethyl carbonate (1/1) solution of $LiPF_6$ (1 M).

Galvanostatic tests were conducted at constant temperature (25 °C) with a Mac Pile controller at discharge rates of 1 Li atom per formula unit in 5 h (denoted *C*/5). GITT (galvanostatic intermittent titration technique) and PITT (potentiostatic intermittent titration technique) experiments were also performed to determine the quasi-equilibrium open circuit potential at various reduction levels in both materials. The OCVs (open circuit voltages) were determined once the time evolution of the voltage was lower than 3 mV/h. Accurate d*x*/d*V* incremental capacities were determined by integrating the chronoamperometric curves recorded for each sample with 10 mV voltage steps and a *C*/20 cutoff limit current.

Results and Discussion

Sample Synthesis and Characterization. X-ray powder diffraction patterns of samples collected along the ball-milling of a stoichiometric Mg/Sn mixture are displayed in Figure 1, that of the sample prepared by simple melting of the same mixture (HT-Mg_2Sn) being added as a reference. Aside from a small amount of metallic tin, the latter sample is found to be a well-crystallized cubic c-Mg_2Sn phase (stable form, JCPDS No. 07-0274), but ground powders appear to be mixtures of c-Mg_2Sn and a metastable high-pressure form of Mg_2Sn referred to as h-Mg_2Sn.[28] Both phases exhibit broad diffraction peaks, indicating a small crystallite size evaluated to be 200 ± 20 Å compared to 600 Å for the as-melt HT-Mg_2Sn material.[29] The crystallite sizes calculated for ground samples are similar for all the crystallographic directions, indicating a general isotropy

(26) Brunauer, S.; Emmett, P. H.; Teller, E. *J. Am. Chem. Soc.* **1938**, *60*, 309.

(27) Morcrette, M.; Chabre, Y.; Vaughan, G.; Amatucci, G.; Leriche, J.-B.; Patoux, S.; Masquelier, C.; Tarascon, J.-M. *Electrochim. Acta* **2002**, *47* (19), 3137.

(28) Cannon, P.; Conlin, E. T. *Science* **1964**, *145* (3631), 487.

(29) Scherrer, P. *Nachr. Göttingen Ges.* **1918**, 98.

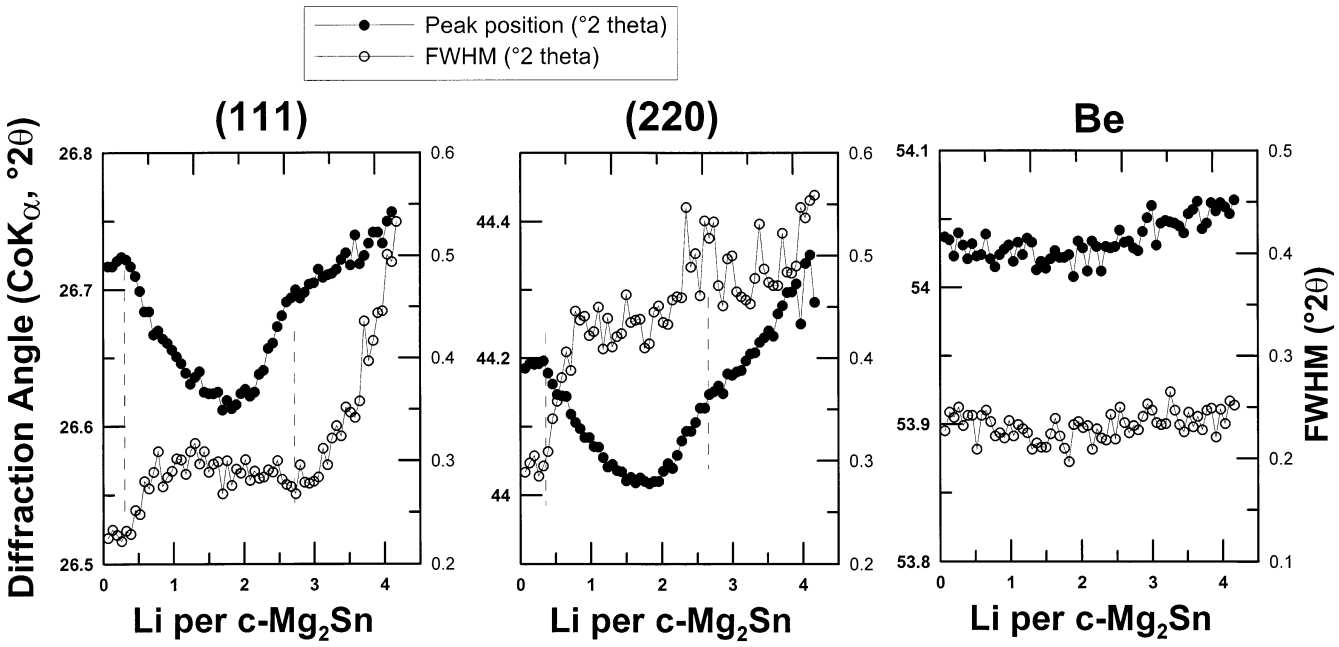

Figure 6. Evolutions in fwhm (empty circles) and position (filled circles) of the (111) and (220) peaks during the discharge of a c-Mg_2Sn/Li cell at 1 Li atom in 5 h at 20 °C. The same evolutions are given for a cell hardware peak (beryllium) as the reference.

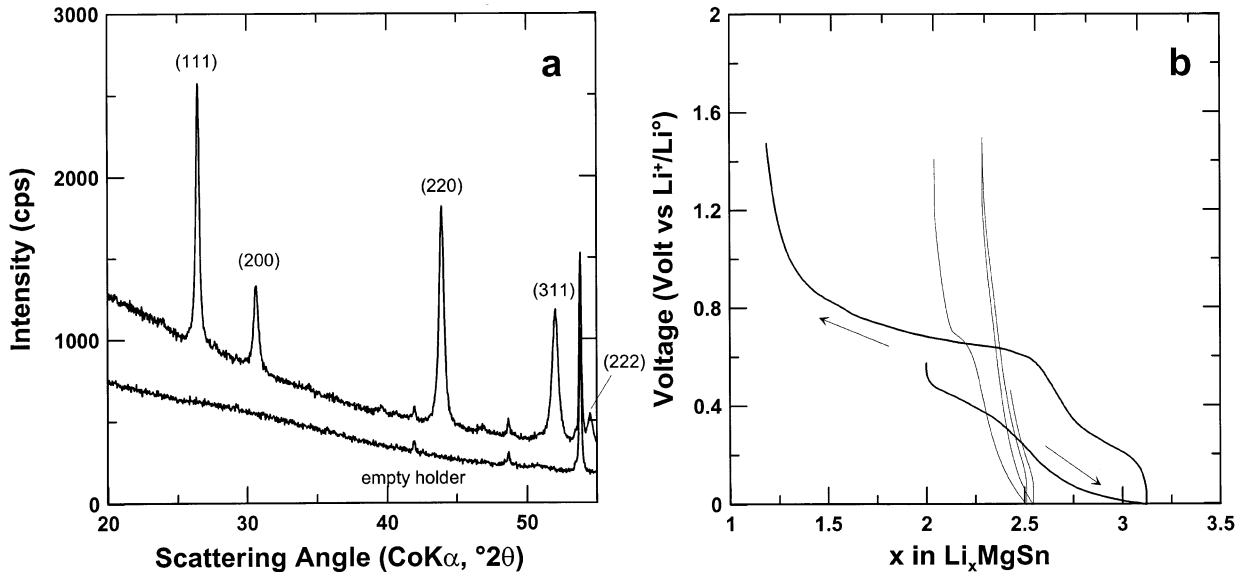

Figure 7. X-ray diffraction patterns of Li_2MgSn powder prepared by ball-milling and that of the empty holder (a) and composition−voltage plot for Li_2MgSn (1 Li atom in 5 h, 20 °C) (b). The equivalent contribution of the conducting SP carbon was computed and superimposed to visualize its contribution to the overall capacity.

in the crystallite shape. As previously reported,[30−32] the proportion of the h-Mg_2Sn phase increases at the expense of that of c-Mg_2Sn as the milling time goes on, and it seems therefore difficult to prepare pure c-Mg_2Sn in that way since both phases are present even after a short milling time. Pure h-Mg_2Sn is obtained after 65 h of milling, with an iron content of around 0.4 atom % (EDS analysis), indicating a negligible contamination from the vial/ball abrasion. The structure of this metastable phase is still questioned,[33,34] but it is well established that it irreversibly converts into c-Mg_2Sn upon mild heating.[30] A batch of c-Mg_2Sn with a small crystallite size was then prepared by heating mill-prepared h-Mg_2Sn for 5 h under vacuum or argon at 350 °C. The resulting powder is made of large particles with sizes ranging from 1 to 20 μm as deduced from SEM observation and is likely nonporous on the basis of the very small BET specific surface area (0.2 m^2/g). From EDS results, the elemental composition of this sample was found to be Mg/Sn = 2.05 ± 0.1, which is very close to the expected value. As for HT-Mg_2Sn, a very small amount of metallic tin is spotted on the XRD pattern of this material (see Figure 1e), but the absence

(30) Urretavizcaya, G.; Meyer, G. O. *J. Alloys Compd.* **2002**, *339* (1−2), 211.
(31) Clark, C. R.; Wright, C.; Suryanarayana, C.; Baburaj, E. G.; Froes, F. H. *Mater. Lett.* **1997**, *33* (1−2), 71.
(32) Sakaguchi, H.; Maeta, H.; Kubota, M.; Honda, H.; Esaka., T. *Electrochemistry* **2000**, *68* (8), 632.
(33) Bolotina, N. B.; Dyuzheva, T. I.; Bendeliani, N. A.; Petricek, V.; Petrova, A. E.; Simonov, V. I. *J. Alloys Compd.* **1998**, *278* (1−2), 29.
(34) Dyuzheva, T. I.; Bendeliani, N. A.; Dzhavadov, L. N.; Kolobyanina, T. N.; Nikolaev, N. A. *J. Alloys Compd.* **1995**, *223* (1), 74.

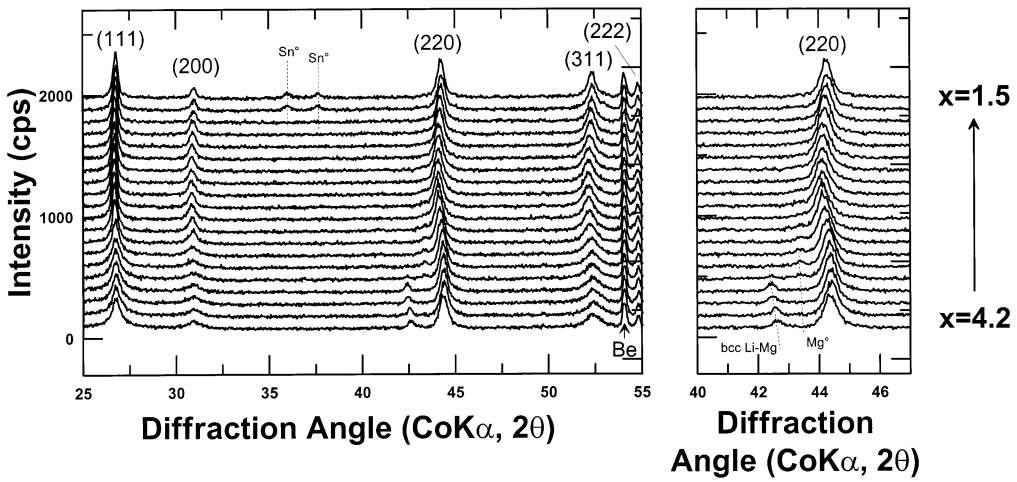

Figure 8. Evolution of the XRD patterns along the charge of a c-Mg_2Sn/Li cell discharged down to 0 V (1 Li atom in 5 h, 20 °C). The beryllium peak is due to the airtight sample holder.

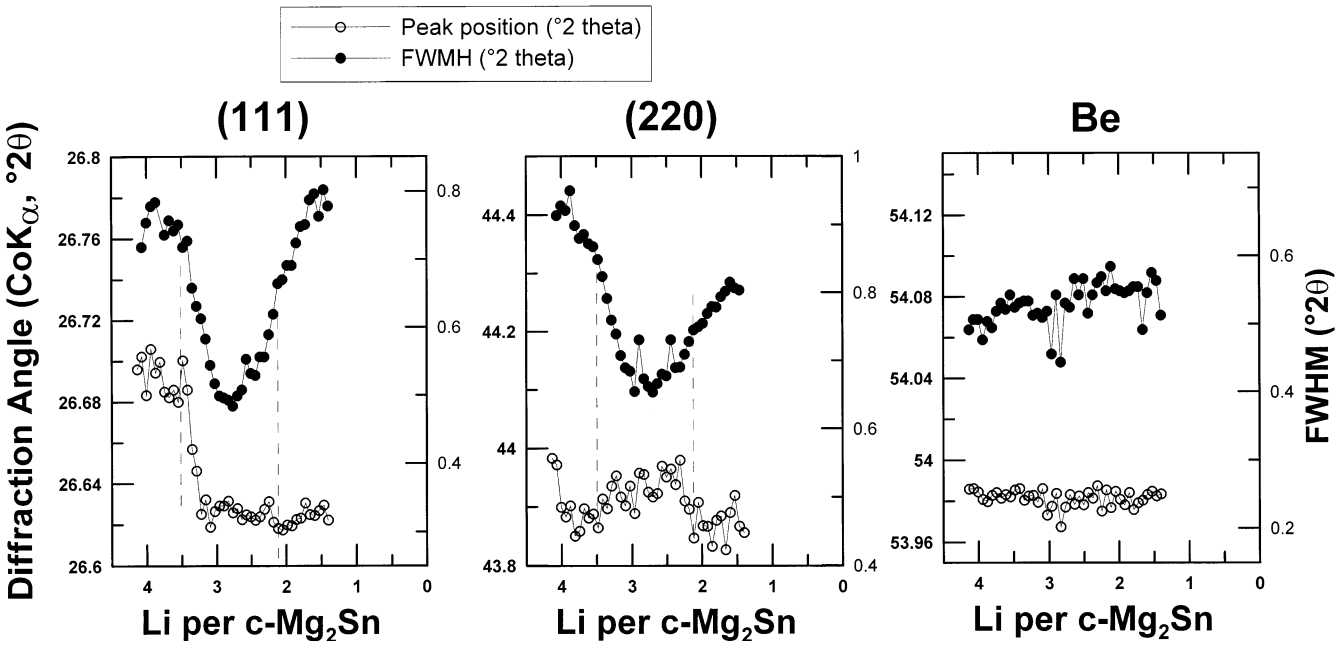

Figure 9. Evolutions in fwhm (empty circles) and position (filled circles) of the (111) and (220) peaks during the charge of a previously discharged c-Mg_2Sn/Li cell down to 0 V (1 Li atom in 5 h, 20 °C). Evolutions are also given for a cell hardware peak (beryllium) as the reference.

of endothermic melting features on the DSC curve (Figure 2) would suggest some possible deviation from the 2/1 ratio in the binary system at elevated temperature. Worth noting is that the Mg−Sn phase diagram consists of a classical two-eutectic congruently melting line-compound system; any deviation from the 2/1 atomic ratio would therefore result in the presence of Sn- or Mg-free metal. The Mg_2Sn phases are known to be slightly reactive with oxygen (and highly reactive toward water as discussed later), and we can suspect some oxide layer growth at the surface of the particles. Such speculation was confirmed by TGA measurements that enable evaluation of the oxide amount to be lower than 2 wt % on the basis of the weight gain of the compound when heated in air up to 800 °C, as compared to the expected theoretical uptake, knowing that the final result is a mixture of MgO and SnO_2.

Electrochemical Characterizations. As a first test, we compared the electrochemical responses of the two Mg_2Sn modifications toward metallic lithium. From galvanostatic cycling curves recorded at a rate of 1 Li atom/5 h for both charge and discharge sweeps (Figure 3), c-Mg_2Sn and h-Mg_2Sn can react with 4.2 and 3.9 Li atoms per formula unit during the first discharge, respectively. The electrochemical signature of the SP carbon is superimposed to show that its contribution to the overall capacity down to 0 V is equivalent to 0.5 Li atom per Mg_2Sn. For both samples, the first discharges consist of a short feature at about 0.7−0.8 V vs $Li^+/Li°$ due to the reaction of Li with additive SP carbon (equivalent to $\Delta x = 0.25e^-$), then a long plateau ($\Delta x = 2e^-$) at 0.25 V (h-Mg_2Sn) and 0.4−0.25 V (c-Mg_2Sn), and finally a low-voltage plateau down to 0 V. To get more accurate data on the process, dx/dV incremental capacities were determined by integrating the chronoamperometric curves for each sample (insets in Figure 3). These plots evidence rather complex and similar discharge signatures with mainly a broad two-peak signal in the 0.35−0.20 V region, a sharp peak at about 0.07−0.08 V, and then a large near 0 V capacity. Aside from the

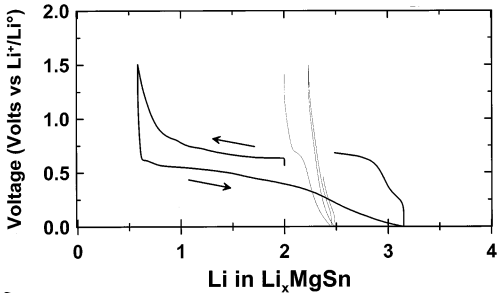

Figure 10. Composition−voltage curve for a Li_2MgSn/Li cell started on charging (1 Li atom in 5 h, 20 °C). The equivalent contribution of the conducting SP carbon was computed and superimposed to visualize its contribution to the overall capacity.

difference in sharpness of the broad signal, both samples behave very similarly. The small discharge voltage plateaus at 0.5 and 0.8 V for c-Mg_2Sn are due to the reaction of lithium with Sn impurity, and correspond to about 0.1 Li atom per Mg_2Sn. These two plateaus accounting for about half of the overall discharge capacity of a Li/Sn cell, the contribution of Sn to the low-voltage Li uptake below 0.5 V vs $Li^+/Li°$ could not exceed 0.1 Li atom per Mg_2Sn. In charging, dx/dV curves also indicate a complex behavior, and exhibit strong similarities between both alloys, implying identical end-of-discharge materials. To further understand these differences and similarities, we conducted in situ XRD experiments while discharging/charging the cells.

c-Mg_2Sn/Li. XRD patterns collected along the discharge of a c-Mg_2Sn/Li cell are shown in Figure 4. Surprisingly, the XRD patterns collected along the first discharge plateau ($\Delta x = 2.7e^-$) do not evidence any important structural changes. This is in good agreement with previously published works[24] pointing out the similarity in the XRD patterns of c-Mg_2Sn and Li_2MgSn. Both phases can be described as a compact fcc network of Sn atoms with all the tetrahedral sites occupied by 8 Mg atoms (c-Mg_2Sn)[35] or 4 Li + 4 Mg ordered atoms (Li_2MgSn).[36] For Li_2MgSn, Li atoms reside in the octahedral sites, while the sites remain available/empty for c-Mg_2Sn (Figure 5). The large difference in the atomic number between Sn and Li/Mg, associated with quasi-identical cubic cell parameters for c-Mg_2Sn (a = 6.7594(4) Å[37]) and Li_2MgSn (a = 6.764(1) Å[36]), result in undistinguishable XRD patterns except for a small difference in intensity for the (200) Bragg peak. In addition, a transformation from c-Mg_2Sn and Li_2MgSn can be facilitated by the existence of a disordered Li_2MgSn phase,[36] undistinguishable from ordered Li_2MgSn by powder XRD, and characterized by a statistical Li/Mg occupation of the tetrahedral sites, where these two elements can thus easily exchange with each other. It was also reported that the $Li_{2-2x}Mg_{1+x}Si$ phases have high Li and Mg conduction properties, further emphasizing the possibility of exchange and mobility in these structures.[38] The first-step discharge overall reaction is as follows:

$$\text{c-}Mg_2Sn + 2Li \rightarrow Li_2MgSn + Mg \qquad (1)$$

In fact, this reaction does not proceed as simply as it appears at first glance. The XRD reflections being quite sharp and well-defined, they could be accurately computed, and Figure 6 displays the evolutions in position and width of the (111) and (220) reflections. The same evolutions are also displayed for a Be reflection (i.e., cell hardware) to discard a possible cell/electrode displacement during cycling. From $x = 0$ to $x = 0.30$, the absence of a change in position/width for c-Mg_2Sn is related to the reaction of Li with additive carbon. Beyond $x = 0.30$, all peaks shift toward lower angle up to a critical concentration, $x = 1.7$, with a resulting overall increase in the cell parameter of only 0.4%. Then, the peaks shift back to high angle up to $x = 2.7$ to reach a position very close to that measured for the initial material. These shifts are associated with a very small broadening of some peaks (e.g., the (111) reflection), while they come with an important broadening of some others (e.g., the (220) reflection). This point is not yet clearly understood, but it nevertheless allows the possibility of a biphasic process involving two phases with very close cell parameters to be ruled out. Indeed, this would have

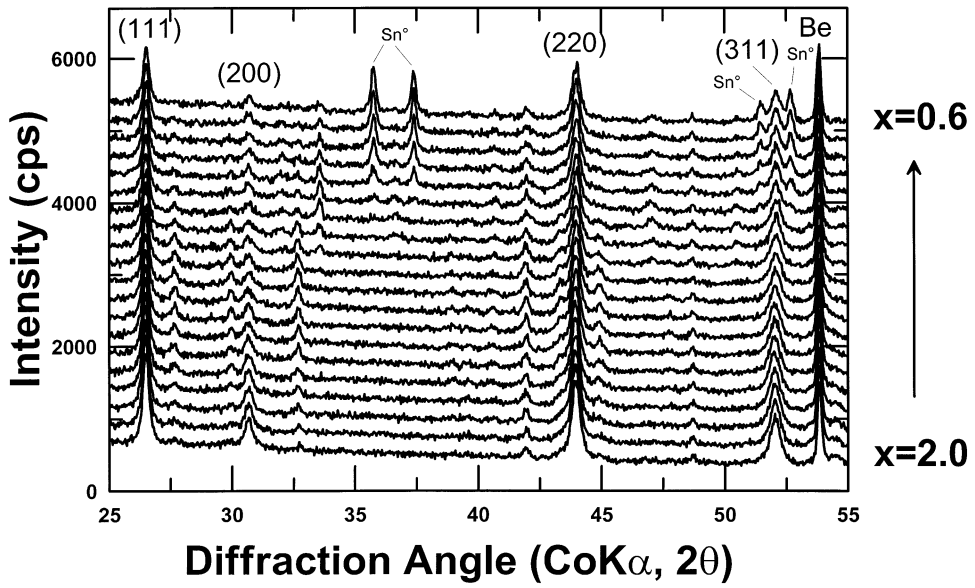

Figure 11. Evolution of the XRD patterns along the charge of a Li_2MgSn/Li cell (1 Li atom in 5 h, 20 °C). The beryllium peak is due to the airtight sample holder.

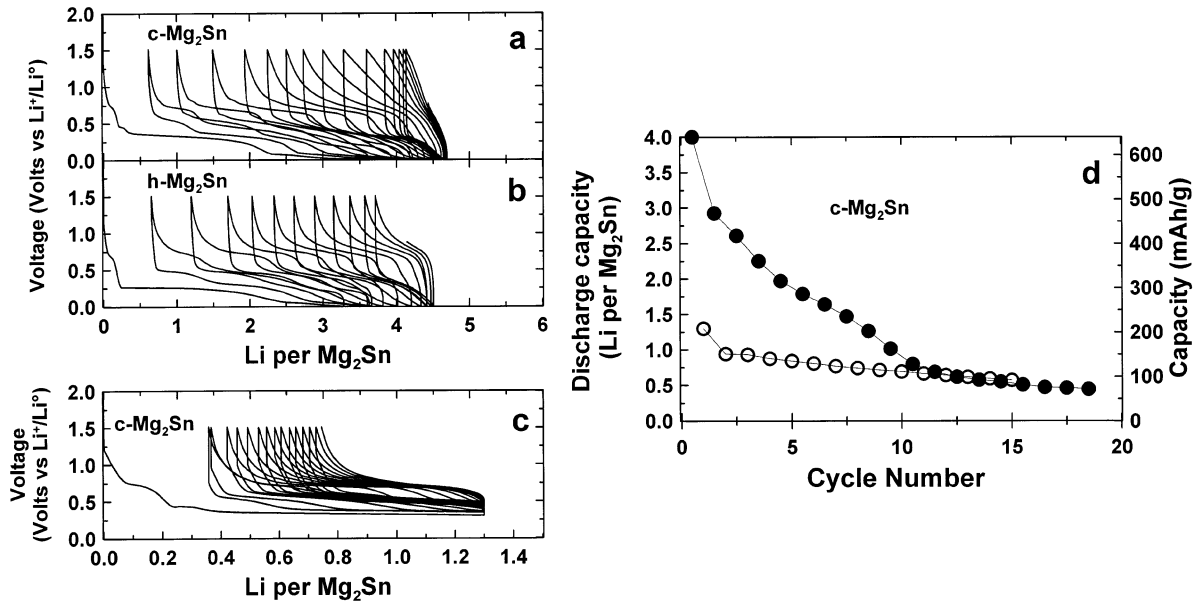

Figure 12. Cycling composition−voltage curves recorded in the 1.5−0.0 V window for c-Mg_2Sn/Li (a) and h-Mg_2Sn/Li (b) cells. (c) displays the cycling composition−voltage curve for a c-Mg_2Sn/Li cell while the maximum reaction extent was limited to $x = 1$ Li atom per Mg_2Sn. The evolutions in discharge capacities for the cells from (a) and (c) as a function of the cycle number are compared in (d). All these data were obtained at a rate of one Li atom in 5 h and at 20 °C.

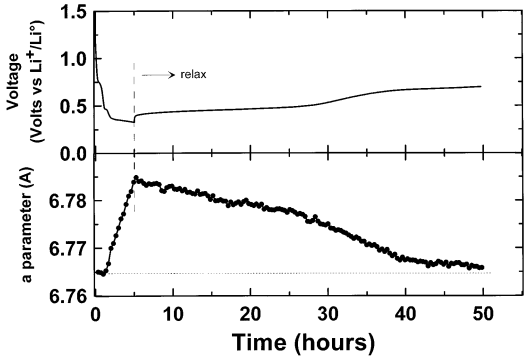

Figure 13. Evolution of the voltage as a function of time during the relaxation of a c-Mg_2Sn/Li cell partially discharged up to $x = 1$ Li atom per formula unit (1 Li atom in 5 h, 20 °C) (top) and simultaneous evolution in the cubic cell parameter of the fcc phase (bottom).

resulted in a reversible apparent broadening of the peak with a maximum width when the two phases had been present in equivalent amounts. Even more interesting is the growth of the (101) Mg° peak at around 2θ = 42.8°, as soon as the critical concentration is crossed, as shown in Figure 4. All these results indicate that the c-Mg_2Sn → Li_2MgSn transformation does not proceed in a simple biphasic way but rather in a two-step transformation as follows:

$$\text{monophasic c-}Mg_2Sn + x_c Li \rightarrow Li_{x_c}Mg_2Sn \quad (1a)$$

$$\text{biphasic } Li_{x_c}Mg_2Sn + (2 - x_c)Li \rightarrow Li_2MgSn + Mg° \quad (1b)$$

The volume expansion linked to process 1a is found to be only 1.3%, while that calculated for reaction 1b is about 30%. One can speculate that reaction 1a corresponds to the filling by Li of the empty octahedral sites of the Sn fcc framework, and that reaction 1b corresponds to the replacement of half of the Mg atoms in tetrahedral sites by lithium atoms concomitantly with Mg expulsion. The successive filling of two types of sites is in agreement with the presence of two features in the dx/dV broad related signal. Nevertheless, this means that the Sn framework is perfectly maintained along the incorporation of Li, Mg acting to some extent as a pillar. This 2-electron reaction is in perfect agreement with the length of the voltage plateau, but additional reaction has to be considered since 4.2 electrons are actually exchanged during the first discharge.

As shown in Figure 4, the XRD patterns collected along the near 0 V feature reveal that the Mg° reflection progressively disappears for the benefit of a new peak located at 2θ = ca. 42.5°. This peak is related to the Li−Mg bcc structure, and its shift toward the position of pure Li with increasing x value is a further indication that we are dealing with a Li−Mg solid solution, as already observed in the case of Mg_2Si/Li cells.[25] The low-voltage capacity can therefore be ascribed to the following reaction:

$$Mg° + xLi \rightarrow Li_xMg \quad (1c)$$

At first sight, this alloying reaction is not supposed to affect the ternary phase. However, from $x = 2.7$ to $x = 4.2$, the peaks of this phase still shift, even if it occurs at a slower pace, and some reflections (e.g., (111)) become much broader (Figure 6). This suggests that the Li_2MgSn phase can have some electrochemical activity at low voltage. To throw some light on this issue, Mg-free Li_2MgSn was prepared by ball-milling elemental metallic powders for 5 h. The absence of free Li (melting point 181 °C) or free Sn (melting point 232 °C) was checked by DSC (Figure 2), and no extra diffraction peak was detected from XRD (Figure 7a). Although this sample is Mg free, its reaction with Li (Figure 7b)

(35) Pauling, L. *J. Am. Chem. Soc.* **1923**, *45*, 2777.
(36) Pauly, H.; Weiss, A.; Witte, H. *Z. Metallkd.* **1968**, *59* (5), 414.
(37) Grosch, G. H.; Range, K.-J. *J. Alloys Compd.* **1996**, *235* (2), 250.

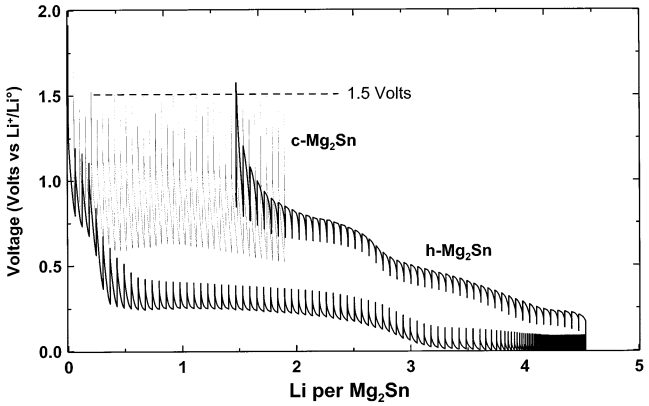

Figure 14. Voltage−composition curves in GITT mode for c-Mg_2Sn/Li and h-Mg_2Sn/Li cells (1 Li atom/5 h, 20 °C). The OCVs at quasi-equilibrium were recorded when the time evolution of the voltage was lower than 3 mV/h.

reveals a nonnegligible low-voltage Li uptake that is evaluated to be 0.5 Li atom per formula unit, once the contribution of the SP carbon is subtracted, and corresponds to the sharp 0.7 V dx/dV peak. For the moment, we have no additional data regarding this process, but this will be a subject of forthcoming diffraction studies. The possibility of electrolyte decomposition at low voltage is unlikely. Indeed, to our knowledge, there is no report of such a reaction for Li/Sn or Li/Mg cells, and the absence of a significant organic-like layer (solid electrolyte interphase) around our particles, as checked by transmission electron microscopy (TEM), definitively rules out this issue.

Upon charging, the evolution of the XRD patterns and peak width and position (Figures 8 and 9) reveal successive processes: (i) a shift of the bcc Li−Mg peak toward low angle and appearance of a shifted (101) Mg° peak; (ii) a reversible peak shift of the cubic Li−Mg−Sn phase, first toward low angle, and then toward high angle, vanishing of the Mg° peak, and sharpening of the fcc Bragg peaks; (iii) growth of a metallic Sn peak.

The first phenomenon is the dealloying reaction of the Li−Mg phase, associated with a voltage plateau, the length of which is smaller (0.5 Li atom) than for the related discharge peak (1.4 Li atoms). This means that this process is partially reversible and that a large part of the Mg remains trapped in Li−Mg alloys:

$$\mathrm{Li}_x\mathrm{Mg} \rightarrow y\mathrm{Mg}^\circ + y\mathrm{Li} + \mathrm{Li}_{x-y}\mathrm{Mg}_{1-y} \qquad (2a)$$

The second phenomenon should correspond to the removal of Li from Li_2MgSn to move back toward Li_{x_c}-Mg_2Sn and c-Mg_2Sn, a reaction that requires the presence of free Mg° to complete the transformation as follows:

$$\mathrm{Li}_2\mathrm{MgSn} + \mathrm{Mg}^\circ \rightarrow \mathrm{Li}_{x_c}\mathrm{Mg}_2\mathrm{Sn} + (2 - x_c)\mathrm{Li} \qquad (2b)$$

$$\mathrm{Li}_{x_c}\mathrm{Mg}_2\mathrm{Sn} \rightarrow \text{c-}\mathrm{Mg}_2\mathrm{Sn} + x_c\mathrm{Li} \qquad (2c)$$

Since the partial reversibility of reaction 2a leads to a limited amount of available Mg ($y < 1$), this process cannot be completed, and the removal of lithium is therefore limited, leading to a $Li_{2-y}Mg_{1+y}Sn$ cubic phase. This explains the shorter associated charge length compared to that of the discharge reaction (1a + 1b), and the smaller amplitude of the shift in peak position upon charging than upon discharging. Note that the (111) peak sharpens along this reaction whereas the width of the (220) peak is not affected.

Finally, the last voltage plateau (0.7 V) surprisingly comes with the formation of metallic tin. This can be understood by the removal of Li from the cubic $Li_{2-y}Mg_{1+y}Sn$ phase, leading to an unstable "$Mg_{1+y}Sn$" phase that transforms into a mixture of stable cubic Mg_2Sn and Sn°:

$$\mathrm{Li}_{2-y}\mathrm{Mg}_{1+y}\mathrm{Sn} \rightarrow (2 - y)\mathrm{Li} + \text{“}\mathrm{Mg}_{1+y}\mathrm{Sn}\text{”} \rightarrow (2 - y)\mathrm{Li} + [(1 + y)/2]\mathrm{Mg}_2\mathrm{Sn} + [(1 - y)/2]\mathrm{Sn} \qquad (2d)$$

This hypothesis was confirmed by looking at the XRD evolution while charging a Li_2MgSn/Li (i.e., no free available Mg) cell up to 1.5 V (Figures 10 and 11). At the end of charging, metallic Sn is indeed observed together with other reflections not yet attributed. Note also the presence of intermediate phases so far not identified. Although only 1.4 out of 2 Li atoms can be removed from the structure, this reaction takes place along a voltage feature at 0.7 V, perfectly matching the voltage observed for reaction 2d. On subsequent dis-

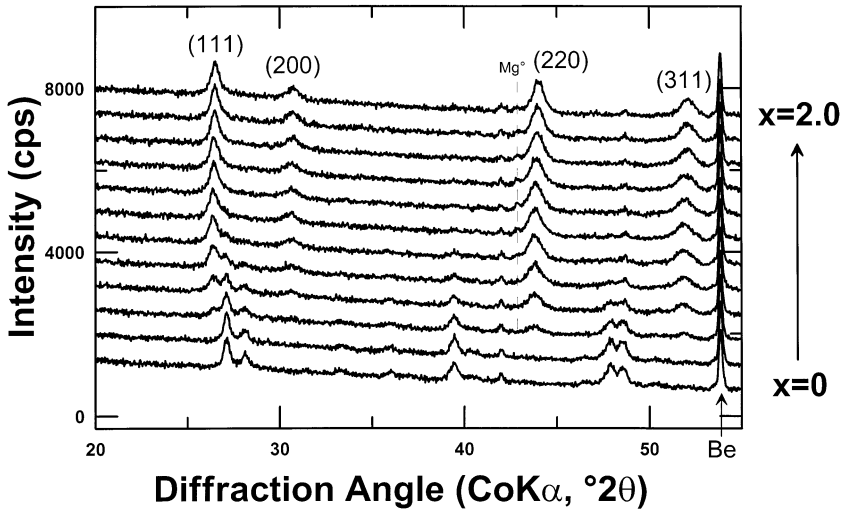

Figure 15. Evolution of the XRD patterns along the discharge of an h-Mg_2Sn/Li cell up to 2 Li atoms per formula unit (1 Li atom in 5 h, 20 °C). The beryllium peak is due to the airtight sample holder.

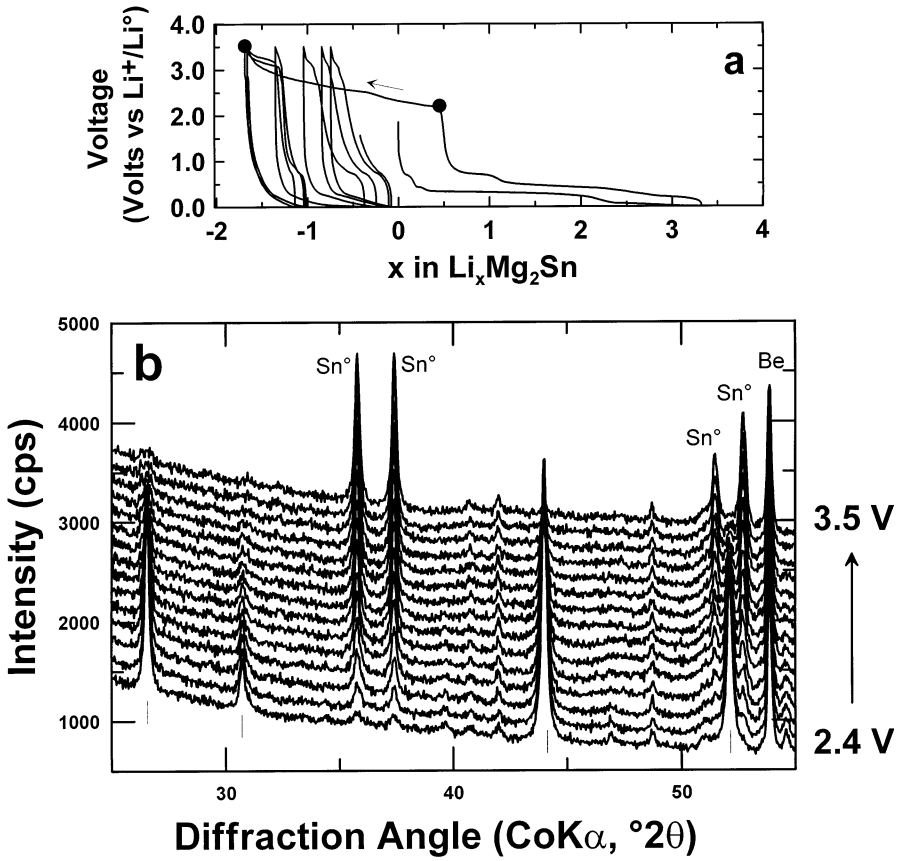

Figure 16. Voltage−composition curve for a c-Mg_2Sn/Li cell cycled in the 0.0−4.0 V range (1 Li atom in 5 h, 20 °C) (a). (b) shows the evolution in XRD patterns during charging at high voltage (voltage >2.4 V). The Be peak is due to the airtight sample holder.

charging, the in situ formed Sn does not react with Li to form Li−Sn alloys as expected, but Li_2MgSn is recovered through a voltage phenomenon at an average voltage of about 0.5 V, nicely matching the new plateau observed along the second discharge for the c-Mg_2Sn/Li cells (Figure 3). Later on, along repeated charge−discharge cycles, the lengths of both plateaus progressively and simultaneously increase, indicating the progressive dominance of these reactions and the progressive loss of available Mg. After a few cycles, the cycling curve for a c-Mg_2Sn/Li cell looks like that of Li_2MgSn/Li, and the capacity decays very quickly (Figure 12a). As observed for Li_2MgSn, the in situ XRD patterns recorded during the second discharge of the c-Mg_2Sn/Li cell show no formation of Li−Sn alloys.[39] This does not come as a surprise since the intimate contact among the Li, Mg, and Sn powders in the milling vials produces a thermodynamically stable ternary phase instead of separate and unstable mixtures of Li−Sn + Mg−Sn.

On the basis of all the previous results, it appears that the expulsion of Mg is detrimental to the reversibility of the processes, first because of the very important volume expansion it involves and second because of the poor reversibility of the formation of Li−Mg alloys. If one limits the cycling to an overall x range of 1.3 Li atoms per c-Mg_2Sn (i.e., formation of Li_1Mg_2Sn and no Mg expulsed), one would expect much better cycling behavior. This is indeed what we observe (Figure 12d), but the cycling curves do nevertheless exhibit increasing capacities at 0.7 V (charge) and 0.5 V (discharge) previously ascribed to reaction 2d (Figure 12c). The only way to explain this unexpected result is an instability of the inserted $Li_{x_c}Mg_2Sn$ confirmed by the evolution of the XRD patterns collected upon relaxation of a fresh cell after being discharged to $x = 1.3$ (Figure 13). As expected, the insertion of Li results in an increase in the cubic cell parameter, but it then decreases as soon as the current is stopped, to monotonically reach a value equal to the initial parameter after about 50 h. Since Li_2MgSn and c-Mg_2Sn phases are known to have the same cell parameters and peak intensities, the following is a possible reaction to account for this observation:

$$2LiMg_2Sn \rightarrow Li_2MgSn + Mg_2Sn + Mg$$

After 10 cycles, only the 0.7 and 0.5 V plateaus are spotted and the material that is submitted to incorporation/removal of lithium is no longer Mg_2Sn, but Li_2MgSn. Actually, $LiMg_2Sn$ is not the only composition to exhibit such instability, but all the intermediate compositions Li_xMg_2Sn ($0 < x < 1$) behave in the same way, and slowly transform into stable mixtures of Li_2MgSn and Mg_2Sn. This is illustrated in Figure 14, where the GITT plot for a c-Mg_2Sn/Li shows a constant quasi-equilibrium voltage (1.5 V) resulting from the biphasic nature of the reaction in these conditions. For the sake of comparison, we simultaneously ran a GITT experi-

(38) Wengert, S.; Nesper, R.; Andreoni, W.; Parrinello, M. *Phys. Rev. Lett.* **1996**, *77* (25), 5083.

(39) Dahn, J. R.; Courtney, I. A.; Mao, O. *Solid State Ionics* **1998**, *111* (3−4), 289.

ment for an h-Mg_2Sn/Li. It took two months for the h-Mg_2Sn/Li to achieve one complete cycle, while the c-Mg_2Sn/Li barely reached $x = 2$ in the same length of time. This means that the time required for c-Mg_2Sn to reach its quasi-equilibrium voltage is much longer than that for h-Mg_2Sn/Li. The quasi-equilibrium voltage is also found to be almost constant when $x < 2$, which is now confirmed in the following section.

h-Mg_2Sn/Li. An in situ XRD experiment for the h-Mg_2Sn/Li cell (Figure 15) along the voltage plateau at 0.25 V evidences a progressive vanishing of the Mg_2Sn Bragg peaks with the concomitant growth of a set of reflections matching the ternary Li_2MgSn cubic phase, without apparent fluctuation in the peak position. This biphasic transformation comes with the expulsion of metallic Mg, the strongest (101) reflection of which is indeed barely observed at $2\theta = 42.8°$. However, the dx/dV plots (Figure 3) indicate that the reaction occurs through distinct phenomena along this plateau. The evolution in XRD patterns along the low-voltage features and upon charging are not shown here as they are similar to what was observed for the cubic phase. These similarities in reaction processes explain why the cycling efficiencies are as poor for the two Mg_2Sn forms (Figure 12b).

High-Voltage Oxidation. A last aspect of the reactivity of these two Mg−Sn alloys is their ability to be oxidized and decomposed at high voltage. This is associated with a long voltage plateau ranging from 2.4 to 3.5 observed either on fresh cells directly started on charging or on cells after one full discharge (Figure 16a). This reaction comes with the growth of metallic tin on the cathode side (Figure 16b), while both Mg (dendrites) and Sn (moss) are recovered on the lithium electrode (EDS analysis). When the charge cutoff voltage is high enough to allow this decomposition reaction to proceed, the cycling behavior is very poor and the growth of dendrites often results in short-circuits of the cells. Note that these dissolution, transport, and metal deposition phenomena are not observed along the 0.7 V charge plateau, where growth of metallic tin also takes place, but through a completely different process. The oxidation of the Mg_2Sn phases mainly occurring below 3.0 V vs $Li^+/Li°$, we could easily check that these phases react with water through release of hydrogen.

Conclusions

By the use of electrochemical titration and in situ X-ray diffraction, we could throw some light on the reaction of Li with Mg_2Sn polymorphs. Although some aspects and steps of the full reaction (i.e., down to 0 V) are still not fully understood, we could nevertheless demonstrate that the reaction of cubic Mg_2Sn takes place successively through (1) a monophasic Li insertion without any metal expulsion, leading to long-term unstable Li_xMg_2Sn phases with a critical concentration close to $x_c = 1$, (2) a biphasic Li insertion into $Li_{x_c}Mg_2Sn$ with Mg extrusion and formation of Li_2MgSn, (3) a possible and limited reaction of Li_2MgSn with Li, and finally (4) an alloying reaction of previously extruded Mg with Li. Upon charging, only a limited amount of Li can be recovered from the Li−Mg alloys, thus forming a small amount of free Mg that limits the charge process to the formation of a $Li_{2-y}Mg_{1+y}Sn$ phase. At higher voltages, lithium can be further extracted from this phase through the formation of Mg_2Sn/Sn mixtures. Along subsequent discharging, Li−Mg−Sn phases are formed, and no Li−Sn alloys can be detected. All these mechanisms lead to very poor cycling efficiency unless the cycling is restricted to a voltage window where the Mg expulsion is avoided. Even so, the performances of these materials are far from being satisfactory for application as electrode materials.

Despite this drawback, the present study demonstrates the complexity of the mechanisms involved in such reactions, and exemplifies that a metallic network can be maintained along full and repeated reactions of insertion and/or displacement. However, the very tiny differences between the XRD patterns for the different phases herein encountered make further analysis or conclusion difficult, and will require complementary studies with other investigation means. This is presently in progress with Mössbauer and neutron diffraction in situ experiments.

Acknowledgment. We thank P. Poizot (LRCS) and P. E. Lippens and J. C. Jumas (LAMMI, Montpellier, France) for sharing their knowledge and for helpful discussions.

CM040132H